

AN INVESTIGATION OF COSMIC GAMMA RAYS

by

PAUL ROBERT HIGBIE

B.A., University of Connecticut
(1958)

SUBMITTED IN PARTIAL FULFILLMENT OF THE
REQUIREMENTS FOR THE DEGREE OF
DOCTOR OF PHILOSOPHY

at the

MASSACHUSETTS INSTITUTE OF TECHNOLOGY

September, 1968

Signature Redacted

Signature of Author
Department of Physics, July 29, 1968

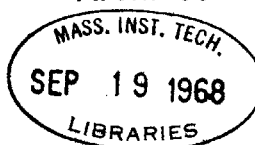
Signature Redacted

Certified by
Thesis Supervisor

Signature Redacted

Accepted by
Chairman,
Departmental Committee on Graduate Students

Archives



AN INVESTIGATION OF COSMIC GAMMA RAYS

by

PAUL ROBERT HIGBIE

Submitted to the Department of Physics on 29th July, 1968,
in partial fulfillment of the requirements for the degree
of Doctor of Philosophy.

ABSTRACT

A celestial anisotropy has been observed by a gamma ray telescope flown on the third Orbiting Solar Observatory. The anisotropy is coincident with the plane of the Galaxy and shows a maximum towards the galactic center. The existence of an isotropic component of high energy gamma rays is also indicated.

Thesis supervisor: George W. Clark

Title: Professor of Physics

ACKNOWLEDGEMENTS

It is a pleasure to thank Professors William L. Kraushaar and George W. Clark for their supervision and many kindnesses shown to me over the past many years. I am deeply indebted to Professor Kraushaar for his long and patient teaching and to Professor Clark for his encouragement these last few months of graduate work.

I also wish to thank Gordon Garmire for many enlightening discussions.

TABLE OF CONTENTS

	Page
Abstract	2
Acknowledgements	3
Table of Contents	4
List of Figures	6
List of Tables	7
I. Introduction	8
A. Historical Remark	8
B. Physical Processes Producing Gamma Rays	9
i. Nuclear Interactions	9
ii. Bremsstrahlung Radiation	10
iii. Inverse Compton Collisions	11
iv. Synchrotron Radiation	12
v. Matter Anti-Matter Annihilation	13
C. Physical Setting for Gamma Ray Processes	14
D. Theoretical Estimates	15
E. Present Experimental Results	16
II. The OSO Instrument	17
A. Description	17
B. Calibration	19
C. The Satellite	21
D. Synopsis of Data Reduction Procedure	23

TABLE OF CONTENTS

	Page
III. Analysis of Data	26
A. High Level Engineering Data	26
B. Consistency Checks for Gamma Ray Events	27
C. Cosmic Gamma Rays	28
D. Conclusions and Suggestions for Further Work	29
Appendix: Calculation of galactic gamma ray luminosity	32
References	34
Biographical Note	36
Figure Captions	37
Figures	39
Tables	56

FIGURES

	Page
1. Integral gamma spectrum from nuclear interactions	39
2. Differential gamma spectrum from nuclear and bremsstrahlung interactions	40
3. Cosmic ray electron intensities	41
4. Integral spectra of inverse Compton radiation	42
5. Schematic of detector	43
6. Geomagnetic variations	44
7. Detector efficiency	45
8. Calibration example	46
9. Photograph of satellite	47
10. Counting rates	48
11. Direction of spin axis	49
12. Accuracy of directions vs. magnetic field	50
13. Earth albedo	51
14. Photomultiplier gains	52
15. Galactic latitude distribution	53
16. Galactic longitude distribution	54
17. Coordinate system for calculation	55

LIST OF TABLES

	Page
1. Flux limits from discrete sources	56
2. Raw data available from satellite	58
3. Quantities calculated or transcribed for each event	60
4. Figures of merit for charged particle effects	61
5. Comparison of spectra observed by the detector	62
6. Predicted and observed directional rates	63

I. Introduction

A. HISTORICAL REMARK

Astronomy has, in recent times, broken out of the traditional visual range of observations and, exploiting new technologies, now encompasses the very long wave length radio domain and the very high energy gamma ray regions. The remarkable discoveries in radio and now radar astronomy comprise a long and well-known story.

Many techniques have been used to examine the range above optical frequencies. Air shower and nuclear emulsion detectors have been used at very high energies. A great variety of counter instruments have been used at lower energies. The first successful -- in the definitive sense of observing an extra-solar, anisotropic source -- such device discovered the Scorpio X-ray source six years ago. Presently, X-ray astronomy is a very rapidly developing field.

This paper is concerned with a particular instrument designed to observe high energy cosmic photons. Its design antecedents lie in the technology developed for accelerator experiments. The energy range applicable, because of its energy response and the generally decreasing energy spectrum expected, is 50 to 500 MeV. This gamma ray detector, aboard the OSO E satellite, has discovered a celestial anisotropy. This discovery inaugurates a fourth observational branch of astronomy: gamma ray astronomy.

B. PHYSICAL PROCESSES PRODUCING GAMMA RAYS

The known mechanisms for producing gamma rays in this energy region are nuclear interactions, bremsstrahlung, inverse Compton, synchrotron radiation, and matter anti-matter annihilations. The first three are probably most important.

i. NUCLEAR INTERACTIONS

Cosmic rays impinging on hydrogen or heavier elements in space can produce mesons and hyperons. Gamma rays are produced as the final products of decay chains leading to π^0 mesons, although there may be a few less important decays such as

$$\Sigma^0 \rightarrow \Lambda^0 + \gamma.$$

The spectrum of π^0 decay gamma rays has a few simple properties. The laboratory energy of the gamma ray is given by the equation

$$E_\gamma = \frac{m_\pi c^2}{2} (1 + \beta_\pi \cos \theta) \gamma_\pi$$

where θ is the angle of emission in the rest frame of a decaying π^0 meson. Since the decay is isotropic in the c.m. $dN_\gamma = d\Omega/2\pi$,

$$\frac{dN_\gamma}{dE_\gamma} = \frac{d(\cos \theta)}{dE_\gamma} = \frac{2}{m_\pi c^2 \beta_\pi \gamma_\pi},$$

$$\text{and } \log E_{\gamma, \max} = \log \frac{m_{\pi} c^2}{2} + \log \sqrt{\frac{1-\beta_{\pi}}{1+\beta_{\pi}}}$$

$$\min$$

which shows that the decay spectrum for a π^0 of given energy is flat and symmetric in a logarithmic plot about $\frac{m_{\pi} c^2}{2}$. Consequently, the spectrum of gamma rays has a maximum at and is symmetric about $m_{\pi} c^2 / 2$ regardless of the original cosmic ray spectrum and independent of the behavior of the cross sections. Of course, this assumes isotropy of the cosmic rays in the source viewed by the observer and this must be kept in mind. For example, the assumption is probably not justified when discussing the earth's albedo.

The gamma ray intensity is then given by

$$I_{\gamma}(E_{\gamma}) = \int dr \int dE_p \sigma(E_{\gamma}, E_p) I_p(E_p, \vec{r}) n(\vec{r}).$$

This integral has been calculated under the assumptions of a homogeneous intensity of cosmic rays and $\langle nL \rangle = 3 \times 10^{21}$ cm by Stecher⁽¹⁾ (fig. 1) and Stecher et al⁽²⁾ (fig. 2).

ii. BREMSSTRAHLUNG RADIATION

Cosmic ray electrons (of both charges) can be formed as the end products of π - μ - e decay chains arising from nuclear interactions of primary cosmic rays with gas, or they can be accelerated via the same route that the nuclear component is. Bremsstrahlung radiation may then be produced by these electrons interacting with the gas. Figure 3 shows the experimentally determined electron fluxes near the earth.^(3,4,5)

Ginzburg and Syrovatskii⁽⁶⁾ estimate the bremsstrahlung spectrum assuming

$$\frac{dN_e}{dE} = 2 \times 10^{-2} E^{-2} e^+ / \text{cm}^2 \text{ sec sr GeV}.$$

They evaluate the integral

$$\frac{dN_\gamma}{dE_\gamma} = M(L) \int_{E_\gamma}^{\infty} \sigma(E_\gamma, E) \frac{dN_e}{dE} dE$$

where $M(L)$ is the mass in gm/cm^2 of the gas along a line of sight to a distance L , under the simplifying assumption that σ is a constant for $E > E_\gamma$ and zero otherwise.

They obtain,

$$\frac{dN_\gamma}{dE_\gamma} = 3 \times 10^{-4} M(L) E_\gamma^{-2}$$

This is plotted in fig. 2 for the same choice of parameters as Stecher made.

iii. INVERSE COMPTON COLLISIONS

Cosmic ray electrons may collide with photons in the ambient radiation field of the galaxy boosting their energy to the gamma ray region. The increase is roughly by the ratio of γ^2 where γ is the Lorentz factor for the electron. So a 100 MeV gamma ray could be produced by a 3.5 BeV electron from starlight or by a 150 BeV electron from the 3°K black body radiation.

If an electron spectrum is again assumed to be $dN_e/dE = kE^{-\alpha}$, the gamma ray spectrum is⁽⁶⁾

$$\frac{dN_\gamma}{dE_\gamma} = \frac{2}{3} N_{ph} k f(\alpha) (m_e c^2)^{1-\alpha} \left(\frac{4}{3} \epsilon\right)^{\frac{\alpha-3}{2}} E_\gamma^{-(\alpha+1)/2}$$

where $\epsilon = 2.7 kT$ is the average black body photon energy, N_{ph} is the number of photons along the line of sight, and $f(\alpha)$ is a slowly varying function of order unity.

Fig. 4⁽⁷⁾ shows a detailed model calculated using the following scheme:

a) The source of cosmic ray electrons is assumed to be homogeneously distributed throughout a disk 1/100 as thick as the radius of the galaxy and the spectral index is a constant.

b) Assuming a confinement time of 10^6 years, taking into account Compton and synchrotron losses an equilibrium solution to the diffusion equation is found.

c) This is then normalized to fit the observed electron spectrum near the earth.

d) The gamma flux due to inverse Compton scattering of the 3°K black body photons by these electrons is calculated.

iv) SYNCHROTRON RADIATION

The characteristic energy, E , for an electron to produce a photon of energy E_γ is given by,

$$E_\gamma = 1.9 \times 10^{-20} H_1 E^2 .$$

If we take H_1 as large as 10^{-5} gauss and E_γ as 50 MeV, then E is 1.5×10^{16} eV. The life time of such electrons is quite short being given by the relation:

$$T_{1/2} = 16.3 m_e c^2 / H_1^2 E,$$

or only 5 years in this case. This mechanism is then almost certainly excluded.

v. MATTER ANTI-MATTER ANNIHILATION

Antiparticles are produced in cosmic ray interactions with the galactic gas so there is at least a trivial production of annihilation gamma rays. If, however, there was a primordial mixture of matter and antimatter the situation may be quite different.

Alfven has proposed a model whose unique features are: first, that matter and antimatter can coexist in the same system; and second, no one would know. The notion is the following. If a cloud and an anti-cloud collide a thin hot layer ("Leidenfrost" layer) is formed by annihilation at the boundary. The kinetic pressure exerted by this hot gas keeps the clouds from interpenetrating farther and so prevents catastrophic annihilation. The rate of annihilation required is so small that gamma radiation (including electron positron annihilation) would not be detected by any present technique. Alfven also suggests that under the influence of a gravitational field a thin "ambiplasma" would precipitate into three

layers: a light ambiplasma of electrons and positrons, a heavy ambiplasma of protons and antiprotons, and -- if the initial ambiplasma were not symmetric -- a layer of pure matter or antimatter. He further calls attention to the common cases of galaxies with two invisible radio regions located on either side, and galaxies with disturbed cores.

C. PHYSICAL SETTING FOR GAMMA RAY PROCESSES

It is certain that all of these processes are to some degree taking place within our galaxy. Cosmic ray electrons and nuclei are directly observed. Radio emission from the electrons is also observed.

There are external galaxies which show various degrees of disturbance. Some of these, in addition to emitting radio waves, emit optical synchrotron radiation. The existence of electrons spiraling in magnetic fields then implies the existence of cosmic ray protons. Disturbed galaxies may also eject material often in the form of two symmetric clouds emitting radio waves.

All these phenomena demonstrate that high energy processes are operative and, consequently, gamma radiation is produced.

The recently discovered quasars, it has been suggested, may involve even higher energy phenomena, e.g. quark interactions.

Finally, if the 3°K radiation is in fact universal and if there are high energy electrons (leaking out of galaxies

for example) in metagalactic space there could then be a diffuse component due to inverse Compton scattering.

D. THEORETICAL ESTIMATES

Each numerical example of the mechanisms discussed above has been calculated for the case of the galaxy. We will content ourselves here to extrapolating these results to extragalactic systems.

Suppose the flux observed at the earth from the galactic nucleus or core is $\phi_{\oplus c}$. Then the rate of production by the core is $N_c = 4\pi \frac{r^2}{w_{\oplus}^2} \phi_{\oplus c}$. The total flux from the disk is, approximately, $N_d = \pi r^2 h S$ where r is the radius of the disk, h its thickness, and S is the number produced per $\text{cm}^3 \text{ sec sr}$. We will make assumptions for ϕ and S based, as will be seen later, on our observations. If we take $\phi_{\oplus c} = 7 \times 10^{-4} \text{ cm}^{-2} \text{ sec}^{-1}$, $S = 5 \times 10^{-26} \text{ cm}^{-3} \text{ sec}^{-1}$, then $N_c = 8 \times 10^{42} \text{ sec}^{-1}$, $N_d = 2 \times 10^{41} \text{ sec}^{-1}$.

For a galactic number density of $N_g = 10^{-75} \text{ cm}^{-3}$ and a Hubble radius of 10^{28} cm we obtain an isotropic flux of

$$F = \frac{N_g N_c R}{4\pi} = 6 \times 10^{-6} \text{ cm}^{-2} \text{ sec}^{-1} \text{ sr}^{-1}.$$

This value is below our observed isotropic flux.

The situation for an hypothesis of metagalactic inverse Compton collisions is illustrated in figure 4. In this case, however, the electrons are assumed to have leaked out of galaxies. The break in the curve corresponds to that energy above which the characteristic energy lifetime of an electron against synchrotron and Compton scattering is less than the diffusion time from the galaxy.

E. PRESENT EXPERIMENTAL RESULTS

Table 1 gives a list of flux upper limits for gamma rays from a number of discrete point sources. (9,10,11)

The best limit, heretofore, to the general isotropic flux of cosmic gamma rays has been that derived from Explorer XI measurements,¹¹ which is $3 \times 10^{-4} \text{ cm}^{-2} \text{ sec}^{-1} \text{ sr}^{-1}$.

II. The OSO Instrument

A. DESCRIPTION

The instrument used in these observations may be called a gamma ray telescope, in the sense that it has a certain crude angular resolution peaked in a single direction. A schematic diagram is illustrated in fig. 5.

The numbers refer to photomultipliers viewing various scintillators in the detector. In order to suppress triggering caused by charged cosmic rays or their secondaries the basic telescope is surrounded by plastic scintillators. Absence of a pulse above a certain threshold in phototubes 8, 9, and 10 viewing the front veto counter for the 1μ sec preceeding or during a certain short interval (τ) is denoted by \bar{A} . \bar{L} denotes the similar case for the top, bottom and side plastics, \bar{B} for the back guard counter. The geometrical opening angle of the telescope is determined by the converter sandwich counter and the energy calorimeter. The former is comprised of four layers of scintillators, two of CsI and two of plastic. Photomultiplier 2 views both a CsI and plastic layer, but the signal from it is electronically separated into two pulses capitalizing on the fact that the time scales for light to be released from plastic and CsI is 3ns and 1.1 μ s respectively. A pulse from either of the last two plastic layers is represented by the logical

symbol $S = \text{true}$.

The energy calorimeter consists of two layers of tungsten and three of NaI. An additional layer of magnesium prevents soft electrons from entering the back guard counter. The calorimeter samples, in a complicated way, the distribution function of the electrons built up in the propagation of a cascade shower through it. The original design attempted to take a more nearly differential sampling of the shower but was limited by statistical fluctuations. The present design will be further discussed below. A pulse from either phototube 4 or 5 then generates true for the symbol T .

Finally, directionality is given to the geometry by the incorporation of a Cerenkov counter (a subsidiary directionality is forced by not incorporating A and B symmetrically in the logic). This counter consists of a lucite radiator viewed by two photomultipliers (6,7) running, for purposes of gain, in "the noise", but in coincidence for a very low accidental rate. The associated logical symbol is C .

A coincidence is said to have occurred between two or more of these signals if they occur within a certain short interval, τ , the resolving time of the system. τ is about equal to $.25 \mu\text{s}$, the longest time constant for the S , C , or T counters, viz. the NaI component.

A master trigger is then,

$$MT = S \cdot C \cdot T \cdot (\bar{A} \cdot \bar{L} + O/D)$$

where O/D is a signal generated during one orbit per day and has the effect of turning off the anticoincidence or veto counters. The information obtained, then, is used for monitoring the gains of phototubes 1 through 5.

If a MT signal is produced information corresponding to an "event" is recorded. Otherwise "routine data" is transmitted during the available telemetry periods. The information available is listed and defined in table 2.

B. CALIBRATION

The efficiency of the front guard counter was measured with sea level cosmic ray μ mesons (a lead absorber was used and the counting rate due to photons and neutrons was checked as a function of its thickness). None of 50,000 μ mesons registered as a gamma ray event.

The intensity of cosmic rays ($\sim .5 \text{ cm}^{-2} \text{ sec}^{-1} \text{ sr}^{-1}$) is then effectively reduced to $10^{-5} \text{ cm}^{-2} \text{ sec}^{-1} \text{ sr}^{-1}$ in competition with a gamma flux of $\eta \phi_\gamma$ where η , the detection efficiency of the telescope for gamma rays, is 8%. This raises the effective competing flux to $10^{-5}/\eta = 1.3 \times 10^{-4} \text{ cm}^{-2} \text{ sec}^{-1} \text{ sr}^{-1}$.

The side counters are about 99% efficient. This was not measured in as great detail as for the front counter, but normal technique would insure at least such a value. Indeed, their effective efficiency is limited to about this

since bolt and cable holes take about 1% of the area screened.

There is a mode of operation for which the \bar{L} requirement is removed (it is later replaced during analysis with information from BLAST). This mode shows a geomagnetic variation (cf. III.B). Hence it is possible for a small fraction of particles coming from the side to undergo reactions complicated enough to produce a false MT. (Fig. 6).

The Cerenkov counter makes the ratio of forward to backward detection efficiencies 300, as measured with μ mesons.

The arrangement of materials in the converter sandwich is for the purpose of distinguishing neutron induced events from gamma events. The nuclear interaction lengths for the CsI and plastic differ considerably from the radiation lengths. The ratio of conversions (CsI to Plastic) is estimated to be 16 for gamma events to 4 for neutrons. The measured ratio for gammas is 13.⁽¹²⁾

Finally, we will briefly discuss calibration of the energy calorimeter and the overall efficiency of the detector.

The instrument was calibrated using a tagged gamma ray beam at the California Institute of Technology. Electrons of known energy were allowed to suffer a bremsstrahlung interaction in a thin target and were then directed by a downstream magnet to focal points conjugate to the target.

The locus of these points is a function of energy of the scattered electrons. Tagging counters placed along this locus provided five energy ranges for the electrons. Making the assumption that multiple photon production is negligible allows one to calculate the energy of the currently tagged gamma ray.

The curve for the efficiency is shown in fig. 7, fig. 8 shows the results for a typical run at a mean gamma ray energy of 365 MeV. The limited statistics for the calorimeter calibration and a disagreement for the albedo flux as measured by Explorer XI, which would hinge on the detection efficiency, has recently led to a decision to recalibrate the instrument.

The working value for the solid area angle factor, Ω , currently used is $0.5 \text{ cm}^2 \text{ sr}$, as defined by the relation

$$\Omega(E) = \int_{4\pi} \int_E^{\infty} \eta(E, \theta) \phi(E) dE d\Omega / 4\pi \phi(>E).$$

Where η is the measured efficiency and ϕ is an assumed flux. The result is rather insensitive to the choice of ϕ ; the number quoted is for $E = 100 \text{ MeV}$. Of course $\Omega(E)$ has real meaning only for E large enough that η is appreciably different from zero.

C. THE SATELLITE

The experiment, one of several on board the Third

Orbiting Solar Observatory, was launched into a near circular, 300 mile high orbit on March 8, 1967. It has been functioning well ever since.

The satellite, fig. 9, consists of two parts; a sail and solar instrument section fixed face onto the sun, and a wheel, rotating at 30 rpm, in which the detector is located looking out along a radius. The detector axis thus slices through the sun every rotation. However, the angular momentum vector, due to magnetic torques and the revolution of the earth, moves about a degree a day. A combination of magnetic torques from on board current coils and gas pulses from the nitrogen stored in spheres on the legs of the satellite keep the spin axis perpendicular to the sun-satellite line and, indeed, allow some positive control over its direction in celestial coordinates. The movement of this axis insures adequate sky coverage for the gamma ray detector.

A magnetometer with its axis lying in plane of the wheel gives a pulse when it lies perpendicular to the component of the earth's field in the plane of the wheel. Since the magnetometer responds to the sense of the field this pulse occurs once per rotation.

A solar sensor is also on board. The lengths of SS, MS, and MM intervals are telemetered in the routine mode. This information, their approximate times of occurrence, the orbital elements of the satellite, accurate representations for the earth's geomagnetic field, and engineering data on

the tilt of the spin axis from the sun-OSO line is combined to give the direction of the angular momentum and its motion in the sky. This, then, with the approximate time of an event and its MTS or MTM suffices to determine the arrival direction of the gamma ray.

D. SYNOPSIS OF DATA REDUCTION PROCEDURE

Once each orbit, as the satellite traverses the radio picket line of receiving stations spaced along the western coast of the Americas, it is interrogated and occasionally issued commands. The satellite responds by telemetering the data accumulated on magnetic tape during its orbit. This data is recorded by the ground station on magnetic tape compatible for initial reduction of NASA's Goddard computer center. At Goddard tapes from the several ground stations are merged according to time sequence and separated according to experimenter.

The experimenters receive tapes which contain the data generated by his own instrument, the universal time for each data frame inserted by NASA on the ground, and flags indicating the quality of radio transmission during segments of the telemetry period.

Several programs were developed at M.I.T. for the analysis of these tapes. The zeroth order step consists of putting the available orbital parameters in a form acceptable to the Pass I program.

In Pass I, the data tapes are used to calculate the

position of the angular momentum vector and, when desired, to produce graphs of the various counting rates for monitoring purposes (fig. 10). An angular momentum example is shown in fig. 11.

The information from Pass I is used in Pass II to calculate the directions of individual gamma events (the entire list of quantities calculated for each event or transcribed from the data tape is listed in Table 3). Also generated is data indicating the intervals for which data was accepted for analysis; the policy being to retain only those intervals for which radio reception was excellent. The output of Pass II is put on magnetic tape in the form of images of punched IBM cards.

The "on time" intervals from Pass II are used to gate the generation of random events in Pass III. This Monte Carlo technique is the heart of the analysis system thus far developed. During an on time period artificial events are generated in such a way that the numbers of events generated during fixed intervals of time give a Poisson distribution with an average rate of 1 in 30 sec. The same quantities are calculated for these events as for the "real" events (except, of course, for pulse heights).

One can set up criteria such as

C = {(mode for gammas only), (geographic coordinates
outside Van Allen belt), (detector axis 40°
above earth's horizon), (geomagnetic latitude

of the satellite less than 20°), (celestial coordinates of the axis in some small bin)}.

The number of artificial events satisfying C is then a statistical measure of the length of time the satellite actually satisfied C . Thus, the ratio of real events under C to the artificial events under C gives a counting rate for this condition.

III. ANALYSIS OF DATA

A. HIGH LEVEL ENGINEERING DATA

The counting rate for the front veto counter (A) is shown as a function of time in fig. 10. The heavy vertical lines correspond to the start of each orbit. The counting rate varies smoothly, corresponding to the expected geomagnetic latitude effect for incoming cosmic rays, except for sudden bursts of very scattered points. These bursts are due to the deep intrusion of the satellite into the Van Allen belt, principally over the South Atlantic magnetic anomaly. Christopher Long has made an empirical fit to several weeks of data excluding these bursts. Although not agreeing with a simple theory which neglects splash and re-enterant albedo and non-uniformity of exposure of the satellite, the fit was considered adequate to determine the Van Allen belt.

A larger portion of data then was examined and the previously determined fit subtracted from it. The residual was plotted for geographic latitude and longitude -- a three dimensional treatment including altitude, considering the circularity of the orbit, would have improved the exposure only marginally -- and regions with the largest accumulation of points were blocked out for the Van Allen criterion.

Internal consistency of the data (and ultimately the production of well-defined maps for earth albedo) is

convincing evidence that the event directions are well known to at least 2° . Comparison of sun and magnetometer determined directions (MTS and MTM) provide a criterion for the magnitude of the magnetic field in the plane of the wheel for use when the satellite is in the earth's shadow. This is necessary since the instant for a zero crossing becomes less accurate and then indeterminate as the field becomes perpendicular. (Fig. 12).

Figure 13 shows the earth's albedo versus the angle of the satellite axis from the horizon. "Sky" events are those with horizon angle larger than 40° .

Figure 14 is a plot of photo multiplier gains for 1S, 2S, F, 3F, 4S, M, 5S. (cf. table 1). The median of the pulse height distribution for charged particles (observed in the O/D mode) is the parameter plotted. The diameter of the points corresponds approximately to their statistical uncertainty.

B. CONSISTENCY CHECKS FOR GAMMA RAY EVENTS

During the time the electronics for the neutron gamma discriminator was working properly there were thirty sky events with a CsI conversion signature and none with a plastic conversion signature. Therefore, sky events are not due to neutrons interacting in the sandwich converter.

As mentioned in II. B there was a mode of operation for the satellite for which the side guard counters were removed from the logic requirement. The counting rate for sky

events shows an increase with increasing geomagnetic latitude, similar to the charged particle flux. So only events with the side counters in the logic were analysed. Fig. 6 shows a comparison of these two modes. The ratio of counting rates for a detector above or below 20° absolute geomagnetic latitude is a figure of merit for interactions caused by particles which could be influenced by the earth's field. Such a list is given in table 4.

C. COSMIC GAMMA RAYS

Figure 15 shows the counting rate as a function of galactic latitude. It is apparent that there is an enhancement towards the galactic plane consistent with the resolution of the gamma ray telescope. This is not to be taken as an average around the disk, however, since the observation time need not be uniform in longitude.

The longitudinal distribution for events within 15° of the plane is shown in fig. 16. If we fit an average rate to the interval outside the range ± 40 we get approximately $F_\oplus = 13 \times 10^{-4} \text{ sec}^{-1} \text{ cm}^{-2}$. The corresponding production rate in the plane is $S = 5 \times 10^{-26} \text{ cm}^{-3} \text{ sec}^{-1}$ (Appendix). Subtracting this from the average within the interval ± 40 yields the value $\phi_{\oplus c} = 7 \times 10^{-4} \text{ cm}^{-2} \text{ sec}^{-1}$ for the flux of photons from the nucleus. These are the values used in providing an estimate for the expected isotropic flux from galaxies (I.D).

If we make a qualitative energy criterion for 4 M,

specifically taking the ratio of the number of events below a certain pulse height to those above, we get the results shown in table 5. We can say, then, that the galactic spectrum is more like the horizon spectrum than the disk spectrum. The disk spectrum is extremely soft; there are many more low pulse height events than large pulse height events compared with the horizon cases. The western horizon has a slightly softer spectrum than the eastern as could be expected since the cut-off momentum for cosmic ray particles is higher towards the east.

One would expect the disk albedo to be quite soft since, to first approximation, the angle of the parent cosmic ray to the observer is always greater than 90° . Any gamma photon produced from π^0 decay at more than 90° in the lab frame has an energy less than $m_\pi c^2/2$. The horizon flux would more nearly correspond to an isotropic distribution -- in the lab frame -- of π^0 decay.

Therefore, the spectrum observed by OSO is consistent with π^0 decay. One cannot go beyond this statement, however, for the spectrum would also be consistent with any of the electromagnetic processes enumerated above. Only an experiment in the 10 to 70 MeV range could clearly differentiate between pure electromagnetic interactions and those caused by initial nuclear interactions.

D. CONCLUSIONS AND SUGGESTIONS FOR FURTHER WORK

What presently can be quoted as an upper limit to an

isotropic component of gamma rays is $10^{-4} \text{ cm}^{-2} \text{ sec}^{-1} \text{ sr}^{-1}$. As is mentioned in II. B this is equal to the effective competing flux of charged particles on the basis of the known anticoincidence efficiency. Thus, the actual existence of an isotropic component depends crucially on the absence of a geomagnetic dependence. Additional argument against a charged particle origin could be made by extending the anticoincidence measurements to 20 weeks.

One might further consider the neutron flux expected from the atmosphere or local production and actually subject the instrument to testing in a neutron beam.

The calibration of the instrument in orbit can be cross checked by examining the horizon events as a function of a characteristic parameter -- i.e. as a function of the cut-off momentum at the horizon along the line of sight.

Table 6 compares the present observations with the predictions of I. B.

These measurements, the local electron energy spectrum, and radio synchrotron emission ought to significantly narrow the range of possible models for electron and magnetic field distribution and, consequently, cosmic ray distributions.

If one accepts the hypothesis that bremsstrahlung or inverse Compton collisions give rise to the observed gamma rays there must be a much larger number of electrons than usually assumed; the radiation field and the gas density are

thought to be well known. Synchrotron radio noise measurements give an upper limit to a product of the galactic magnetic field and the electron density. Consequently, the field is reduced and the leakage time for electrons and cosmic rays is also reduced.

Supernova explosions barely have been able to account for the abundance of cosmic rays using arguments on energy balance. The chemical composition and isotropy of cosmic rays provide limits on their diffusion, if a supernova origin is assumed, and the rate of supernova outbursts is estimated from historical sources or statistical studies of observed outbursts in external galaxies.

The gamma ray observations reported here provide another constraint for models of cosmic ray and electron distributions in the galaxy. It is felt that further study of the efficiency of cosmic ray generation by supernovae is needed.⁽¹³⁾ Also, the possibility should be investigated that gravitationally collapsed objects,^(14,15) which may be common in the galaxy,⁽¹⁶⁾ could play a role in these phenomena.

APPENDIX

The longitude distribution (fig. 17) for the region $|l^{\text{II}}| > 40^\circ$ can be approximated by a constant $1.41 \times 10^{-4} \text{ sec}^{-1}$. A χ^2 test that a constant counting rate is appropriate gives a probability of 30% that greater fluctuations would be seen in repeated observations ($\chi^2 = 15.10$ for $F = 13$). Subtracting the average rate for $|b^{\text{II}}| > 30^\circ$, $.56 \times 10^{-4} \text{ sec}^{-1}$, and using the instrument's geometrical factor of $0.4 \text{ cm}^2 \text{ rad}$ one obtains $2.1 \times 10^{-4} \text{ cm}^{-2} \text{ sec}^{-1} \text{ rad}^{-1}$ for the average strength of the galactic plane considered as a line source. The excess counts from the region towards the galactic center then give a flux of $6.7 \times 10^{-4} \text{ cm}^{-2} \text{ sec}^{-1}$.

Let S be the production rate of gamma radiation per unit volume. Assuming it is constant throughout the disk, the total observed flux would be,

$$F_{\oplus} \approx \int d\varnothing \int_{\rho_0}^R \frac{S}{\rho^2} h \rho d\rho,$$

where $R = \sqrt{r^2 - \bar{w}_{\oplus}^2 \sin^2 \varnothing} + \bar{w}_{\oplus} \cos \varnothing$ (Fig. 17), h is the thickness of the disk, and ρ_0 is the distance for which the assumption of a thin lamina breaks down. The terms in \varnothing fortuitously cancel and,

$$F_{\oplus} \approx \pi S h \ln \frac{r^2 - \bar{w}_{\oplus}^2}{\rho_0^2}$$

Setting $F_{\oplus} = 2\pi(2.1 \times 10^{-4}) = 1.3 \times 10^{-3} \text{cm}^{-2} \text{sec}^{-1}$,
 $r = 15 \text{ kpc}$, $\bar{w}_{\oplus} = 10 \text{ kpc}$, $h = .5 \text{ kpc}$, and $\rho_0 = h/2 \tan 15^\circ$
gives $S = 5.3 \times 10^{-26} \text{cm}^{-3} \text{sec}^{-1}$.

REFERENCES

1. Stecher, F. W., Smithsonian Astrophysical Observatory
Special Report 260, (1967).
2. Stecher, F. W., S. Tsuruta, and G. G. Fazio, *Astrophys.*
J. 151, 881-94, (1968).
3. Anand, K. C., R. R. Daniel, and S. A. Stephens, *Phys.*
Rev. Letters, 20, 764-8, (1968).
4. Israel, M. H., and R. E. Vogt, *Phys. Rev. Letters*, 20,
1053-6, (1968).
5. Fanselow, F. L., *Astrophys. J.*, 152, 783-99, (1968).
6. Ginzburg, V. L. and S. I. Syrovatskii, The Origin of
Cosmic Rays, Pergamon Press, New York, 1964.
7. Shen, C. S., and G. Berkey, *Astrophys. J.*, 151, 895-900,
(1968).
8. Alfven, H., *Rev. Mod. Phys.*, 37, 652-66, (1965).
9. Frye, Jr., G. M., F. Reines, A. H. Armstrong, *J. Geophys.*
Res., 71, 3119-24, (1966).
10. Fichtel, C. E., and D. A. Kniffen, *J. Geophys. Res.*, 70,
4227-34, (1965).
11. Kraushaar, W. L., G. W. Clark, G. Garmire, H. Helmken,
P. Higbie, and M. Agogino, *Astrophys. J.*, 141,
845-63, (1965).
12. Gordon Garmire, private communication.
13. Colgate, S. A., and R. H. White, *Astrophys. J.*, 143,
626-681, (1966).

14. Harrison, B. K., K. S. Thorne, M. Wakano, J. A. Wheeler,
Gravitational Theory and Gravitational Collapse,
University of Chicago Press, (1965).
15. Penrose, R., Phys. Rev. Letters, 14, 57-59, (1965).
16. Woltjer, L., Lectures in Galactic Dynamics Given at
Massachusetts Institute of Technology 1962/63.

BIOGRAPHICAL NOTE

Paul R. Higbie was born on October 5, 1937 in Makati Rizal on the Philippine Islands. He attended primary and secondary schools in Virginia, Rhode Island and Connecticut. In 1958, he received the degree of Bachelor of Arts from the University of Connecticut where he was named University Scholar and was graduated with highest honors in physics. He entered the Graduate School of Massachusetts Institute of Technology in 1958. Prior to the completion of graduate studies, he was employed as a technical assistant on the Explorer XI experiment at M.I.T. under Professors William L. Kraushaar and George W. Clark.

In 1965 he married Miss Virginia C. Francis of New Bedford, Massachusetts. They have two children, Jennifer and David.

FIGURE CAPTIONS

- Fig. 1. Integral gamma ray spectrum calculated from known p-p interaction cross-sections.
- Fig. 2. Differential gamma ray spectrum, including the data of fig. 1 and results from pion production models at higher energies.
- Fig. 3. Differential cosmic ray electron fluxes observed near the earth. Typical error bars are shown.
- Fig. 4. Integral spectra of inverse Compton radiation. The calculation has been done for a model in which the electrons are mainly confined to the plane.
- Fig. 5. Schematic of the detector.
- Fig. 6. Geomagnetic variation of the apparent gamma ray rate with the side guard counters off and on.
- Fig. 7. The efficiency of the detector as a function of energy for radiation incident along its axis and at 15° to it.
- Fig. 8. Pulse height distributions for a typical calibration run.
- Fig. 9. Picture of the satellite sheltering the gamma ray detector. The vertical semi-circular structure, called the sail, is maintained face onto the sun.
- Fig. 10. Example of the routine sampling of various counting rates in the instrument. The line labeled A corresponds to the front plastic.

FIGURE CAPTIONS

- Fig. 11. Example of the daily variations in the direction of the angular momentum vector.
- Fig. 12. Correspondence between the difference between the sun and magnetometer determined directions versus the magnetic field in the plane of the wheel. The median and 90th percentile angles for the distribution of cases for each value of the magnetic field are plotted.
- Fig. 13. Earth albedo showing cut-off for sky events.
- Fig. 14. Plots of photomultiplier gains. The slight rise for 2 S occurs when the neutron-gamma discriminator was functioning properly.
- Fig. 15. Galactic latitude variation.
- Fig. 16. Galactic longitude variation for events with galactic latitude less than $\pm 15^\circ$.
- Fig. 17. Coordinate system used for calculation described in appendix.

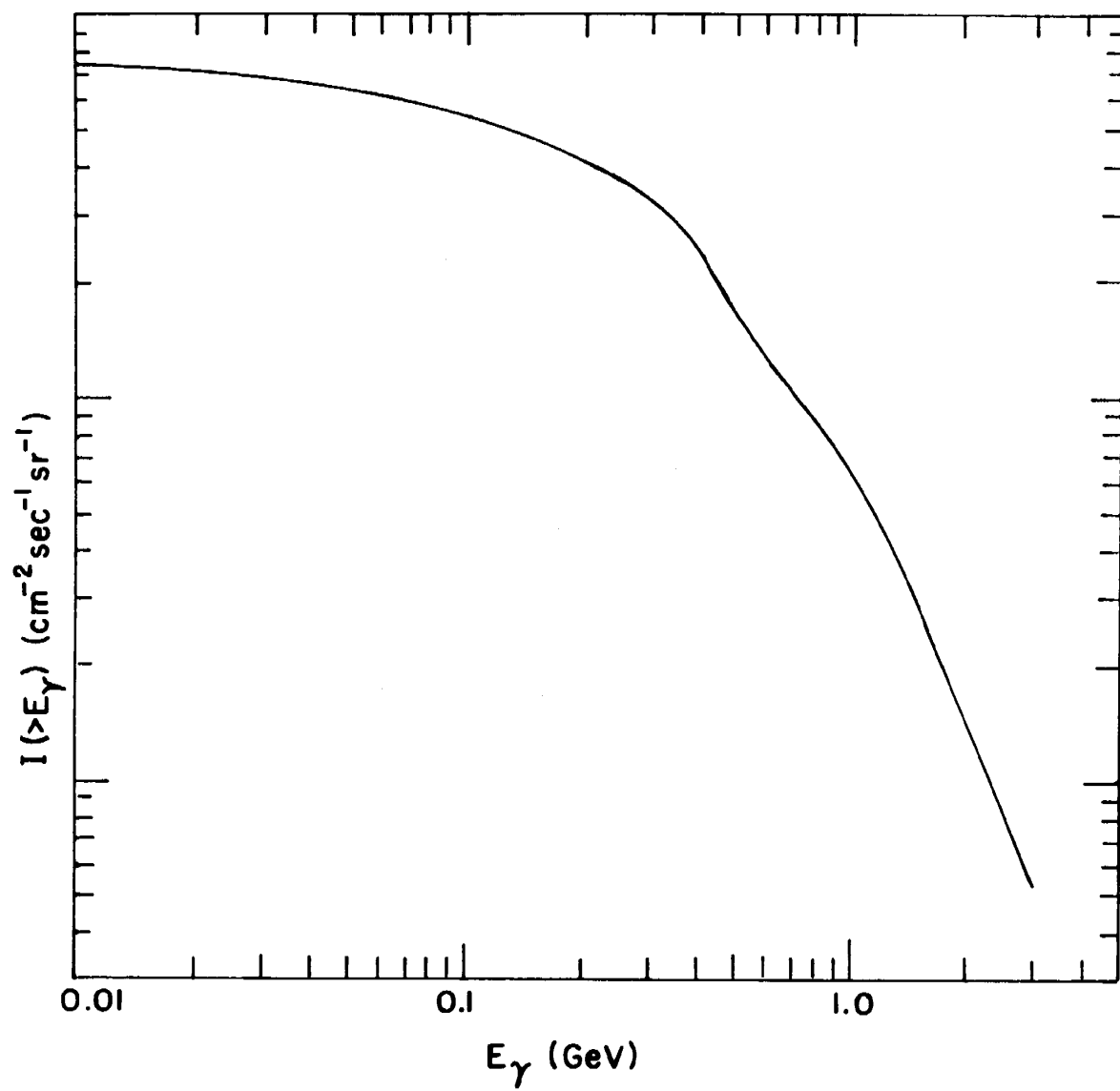


Fig. 1

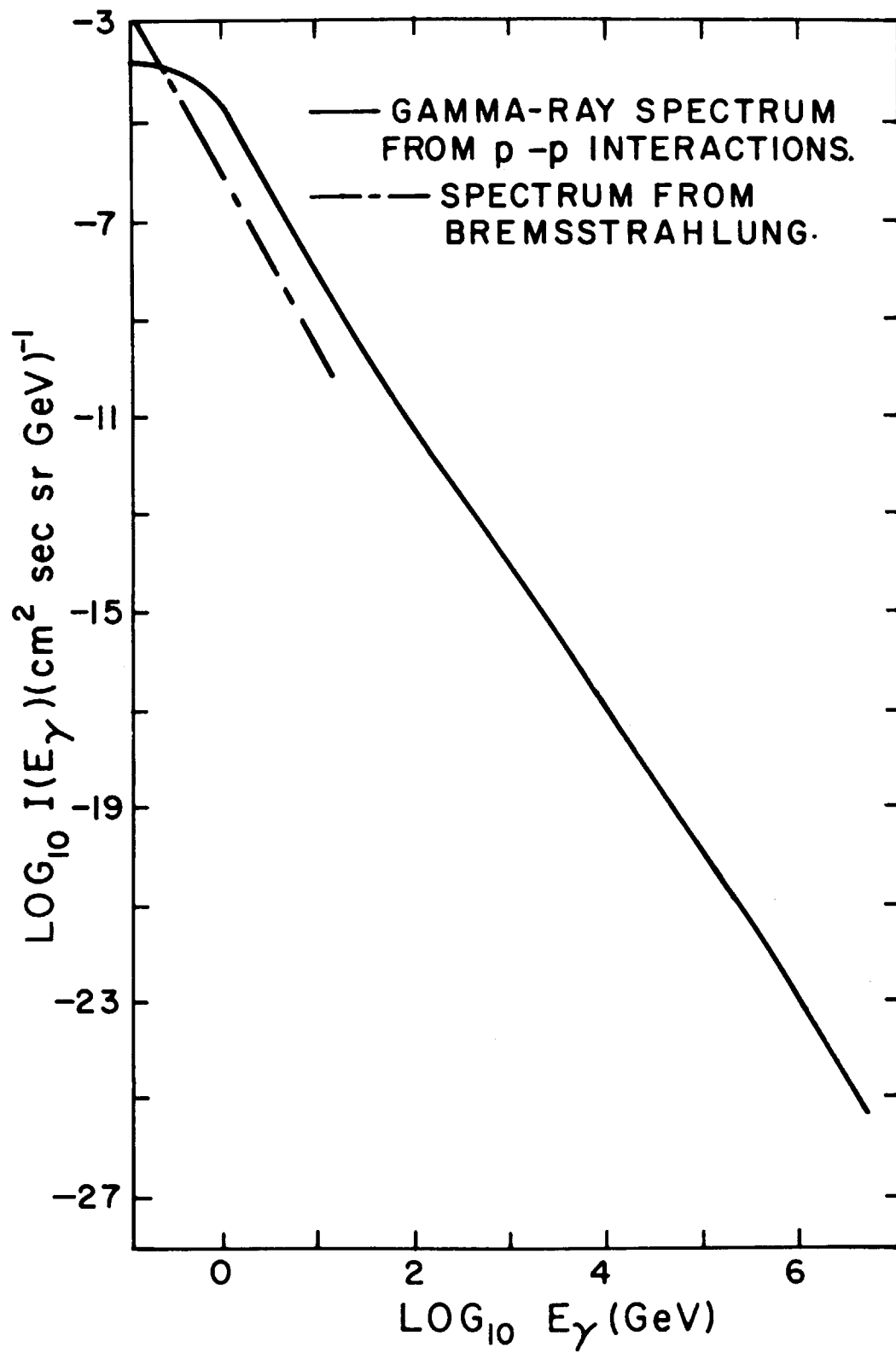


Fig. 2

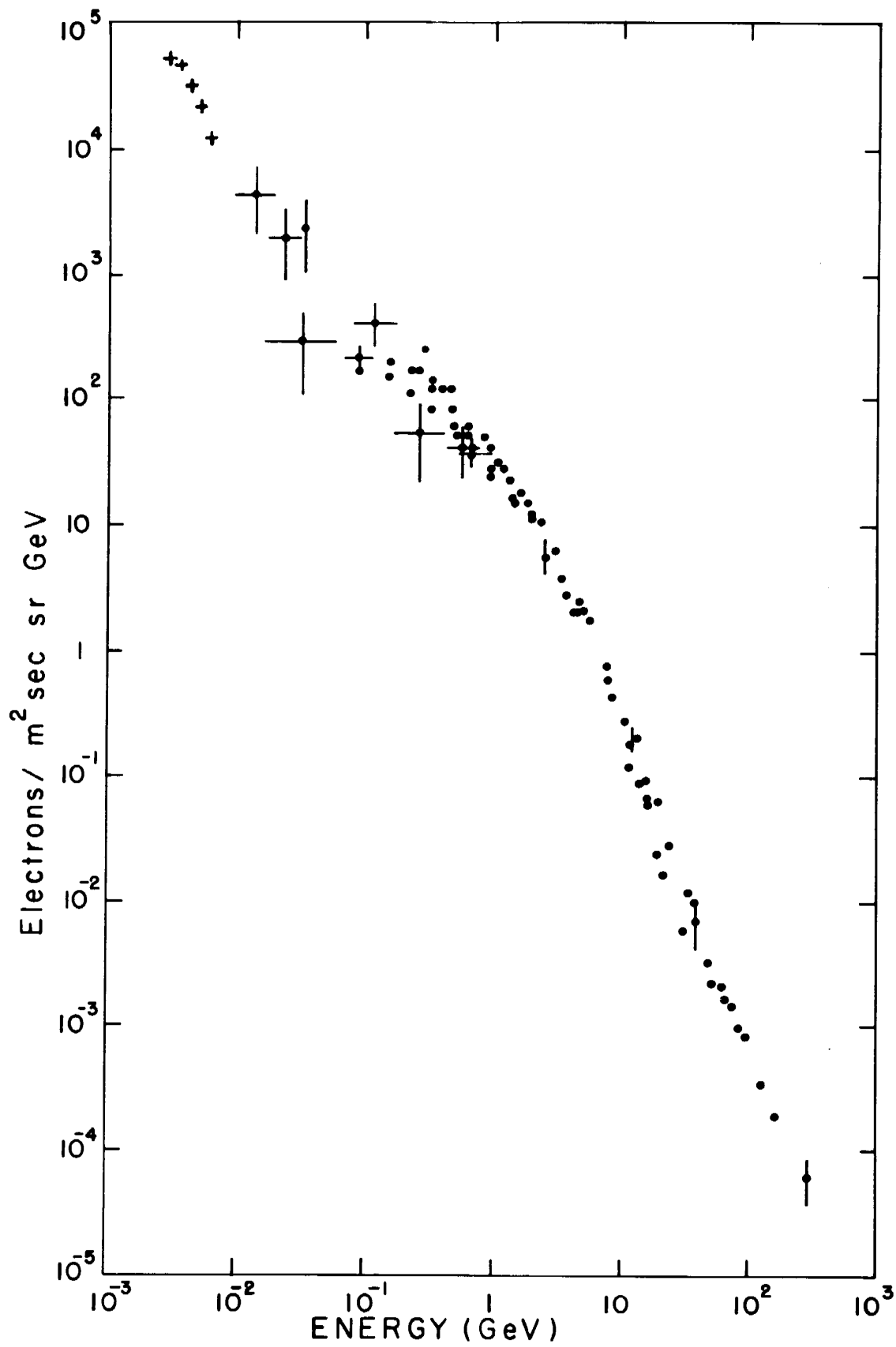


Fig. 3

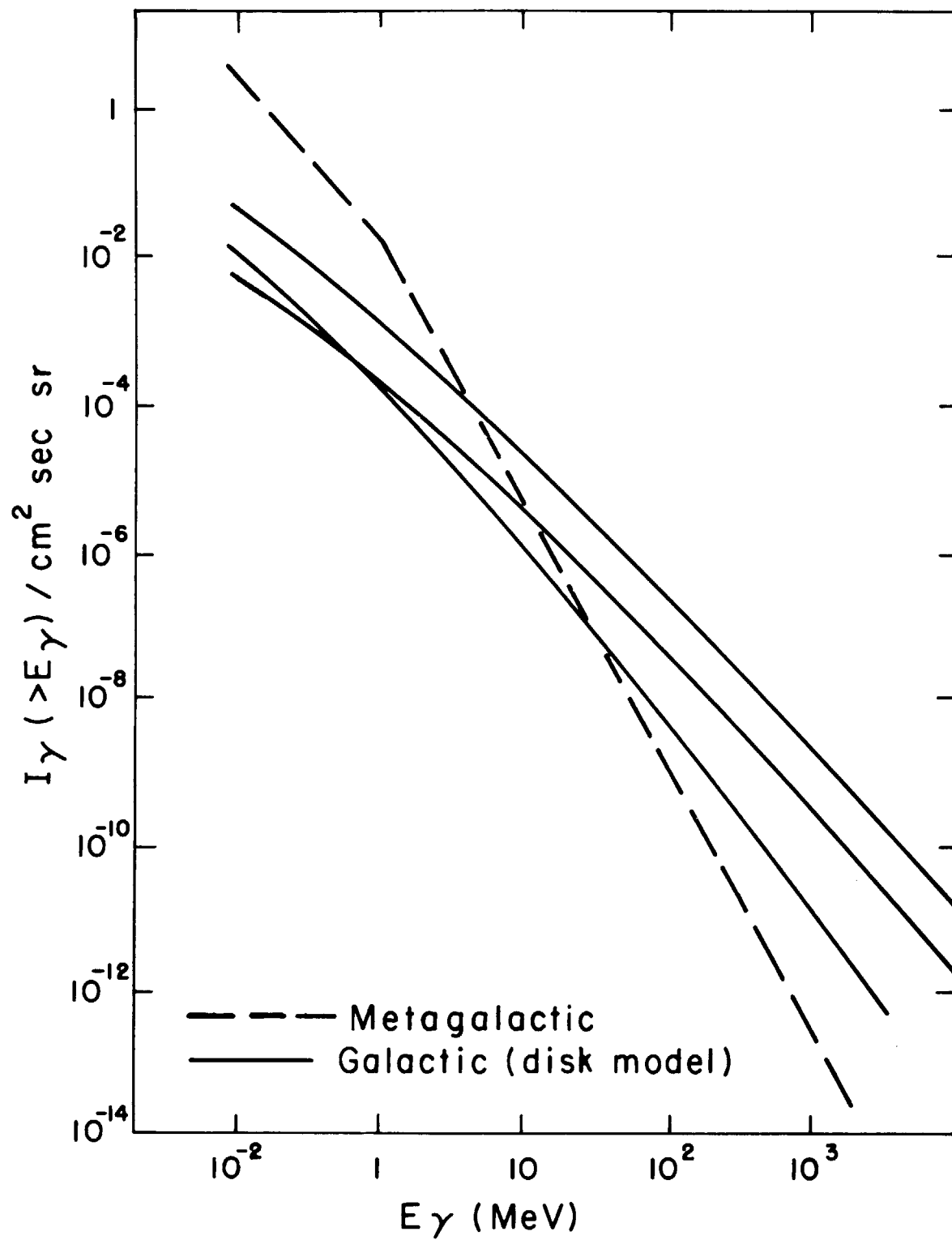


Fig.4

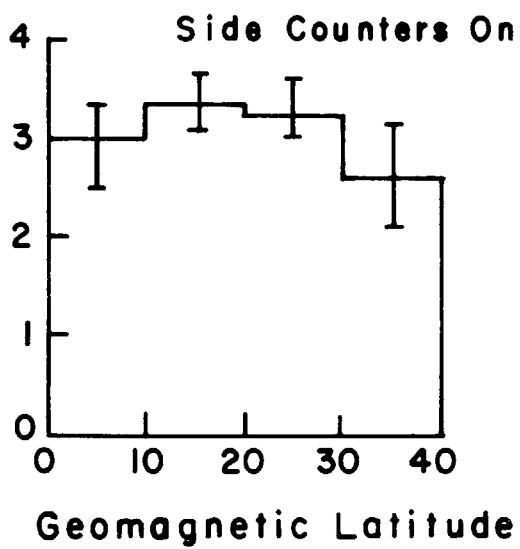
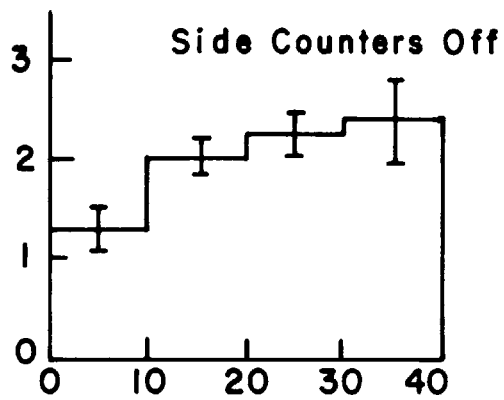


Fig. 6

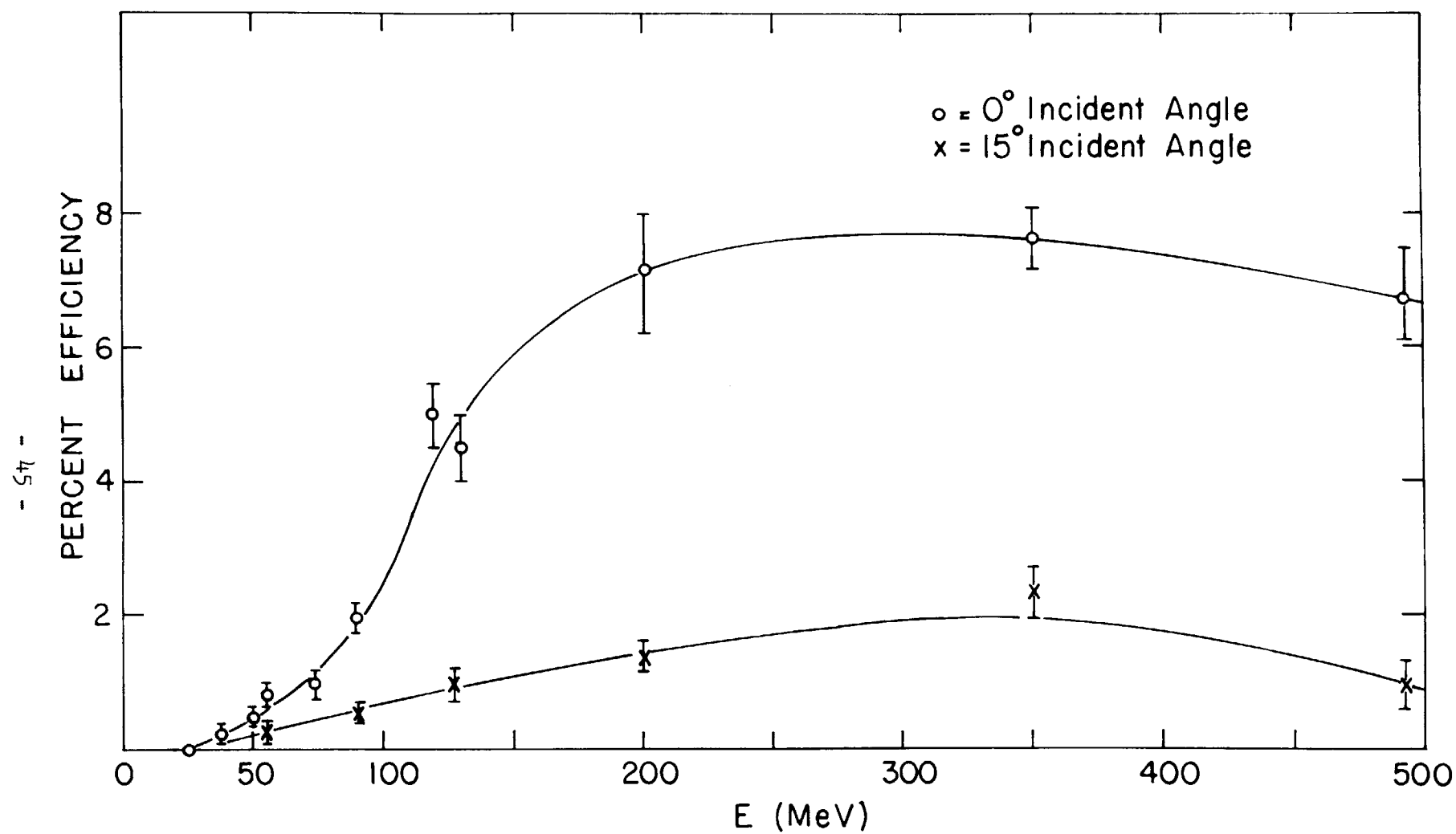
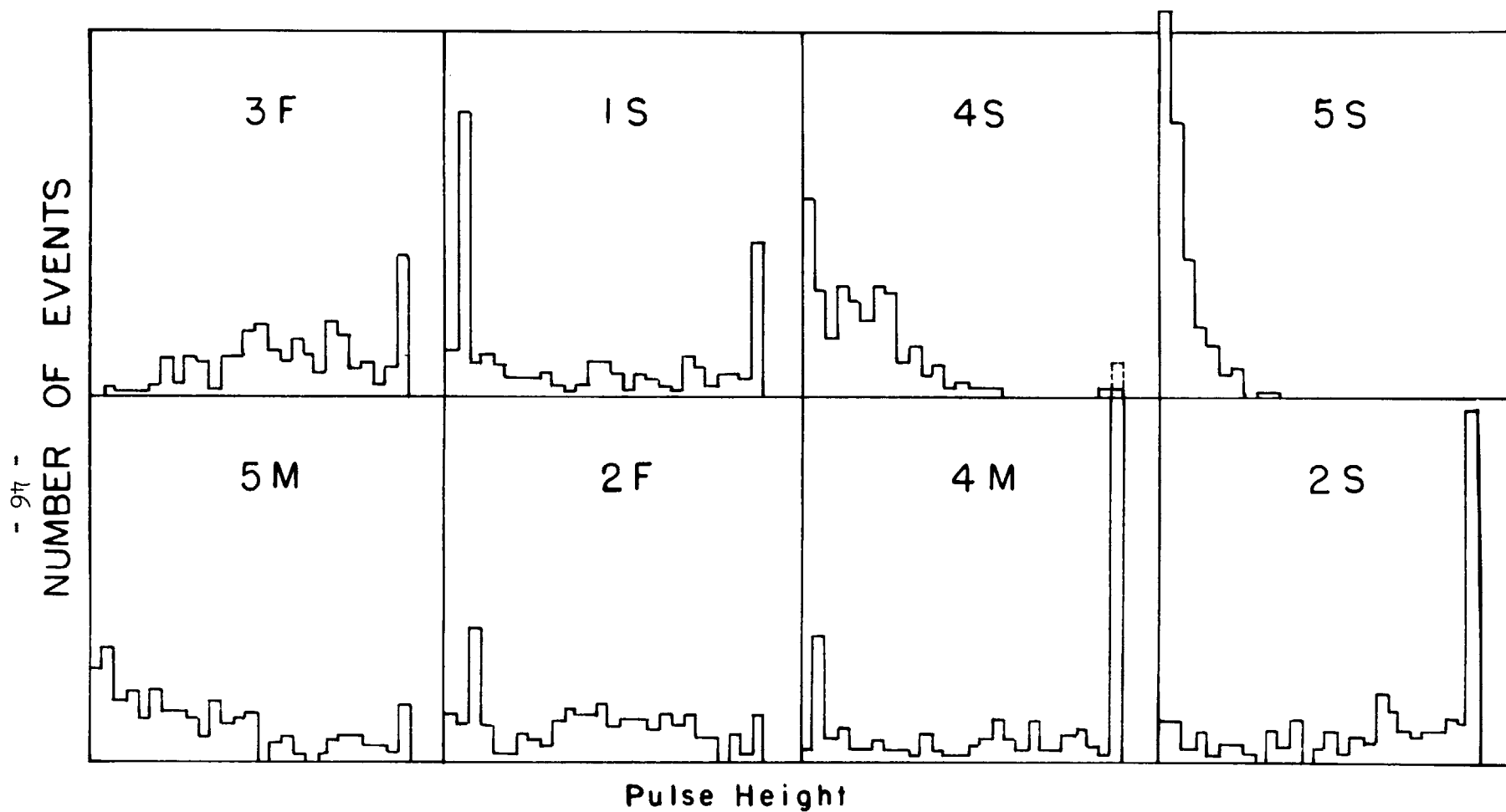


Fig. 7



PULSE HEIGHT MEASUREMENTS

Fig. 8

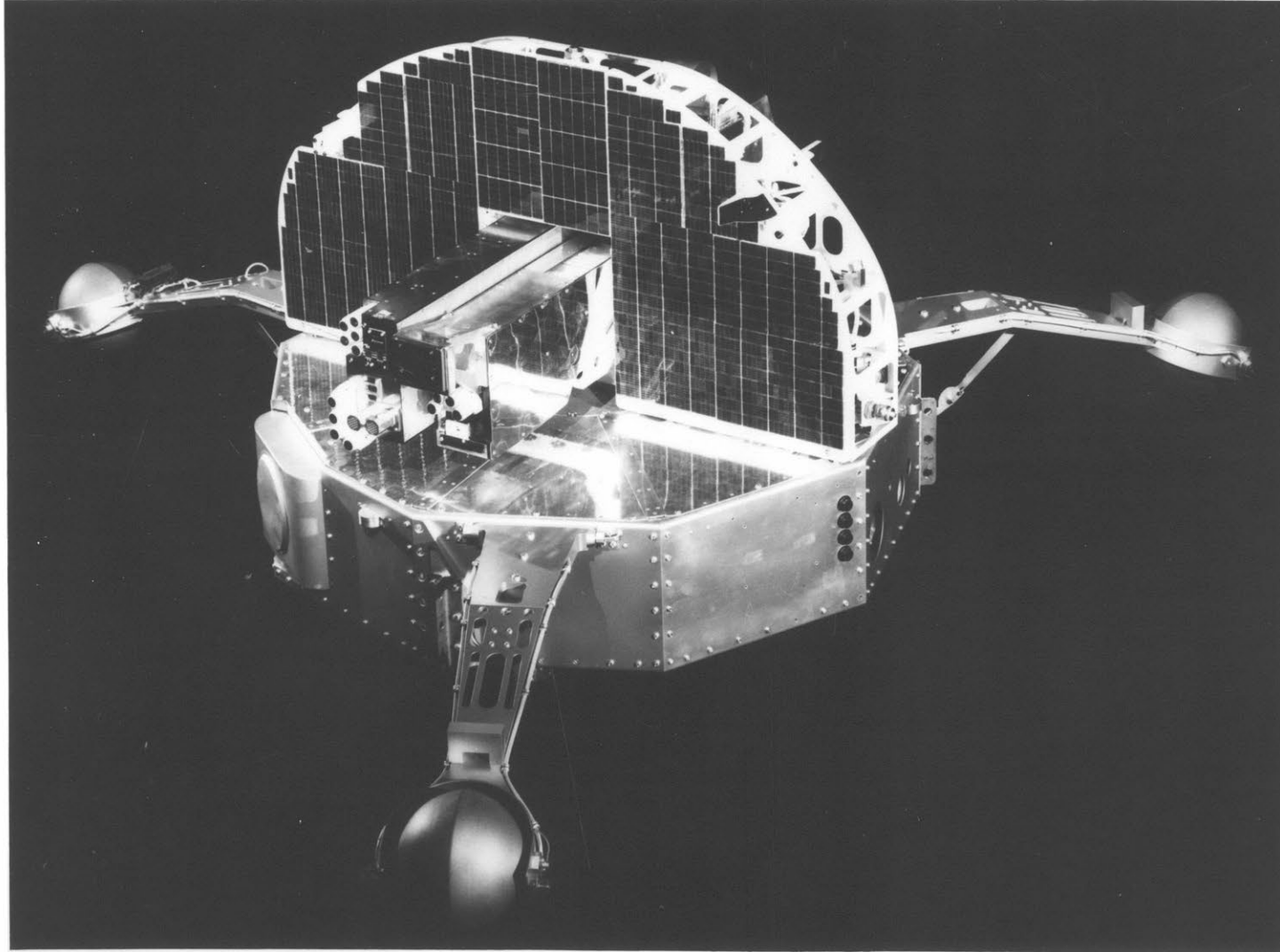


FIG. 9

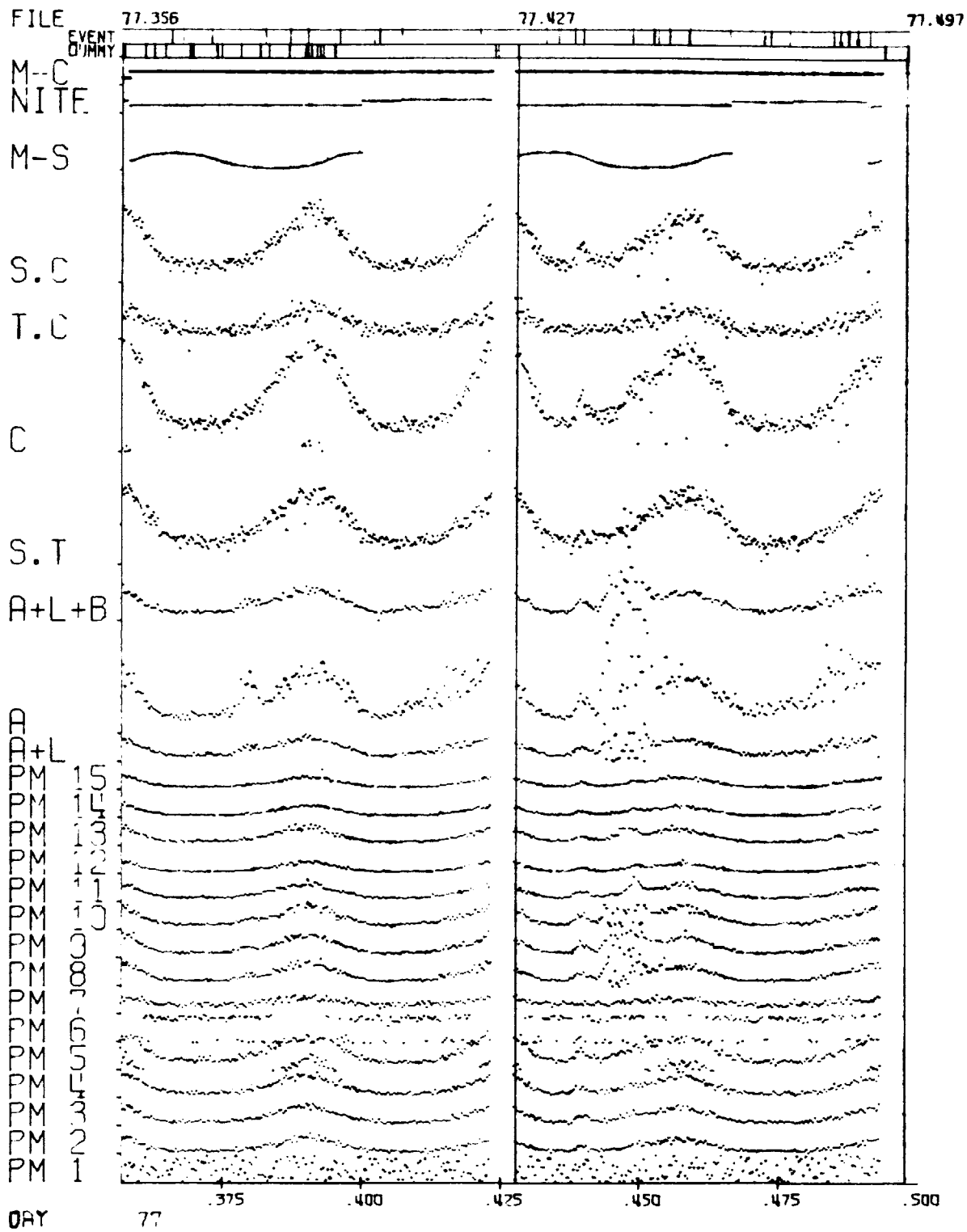


FIG. 10

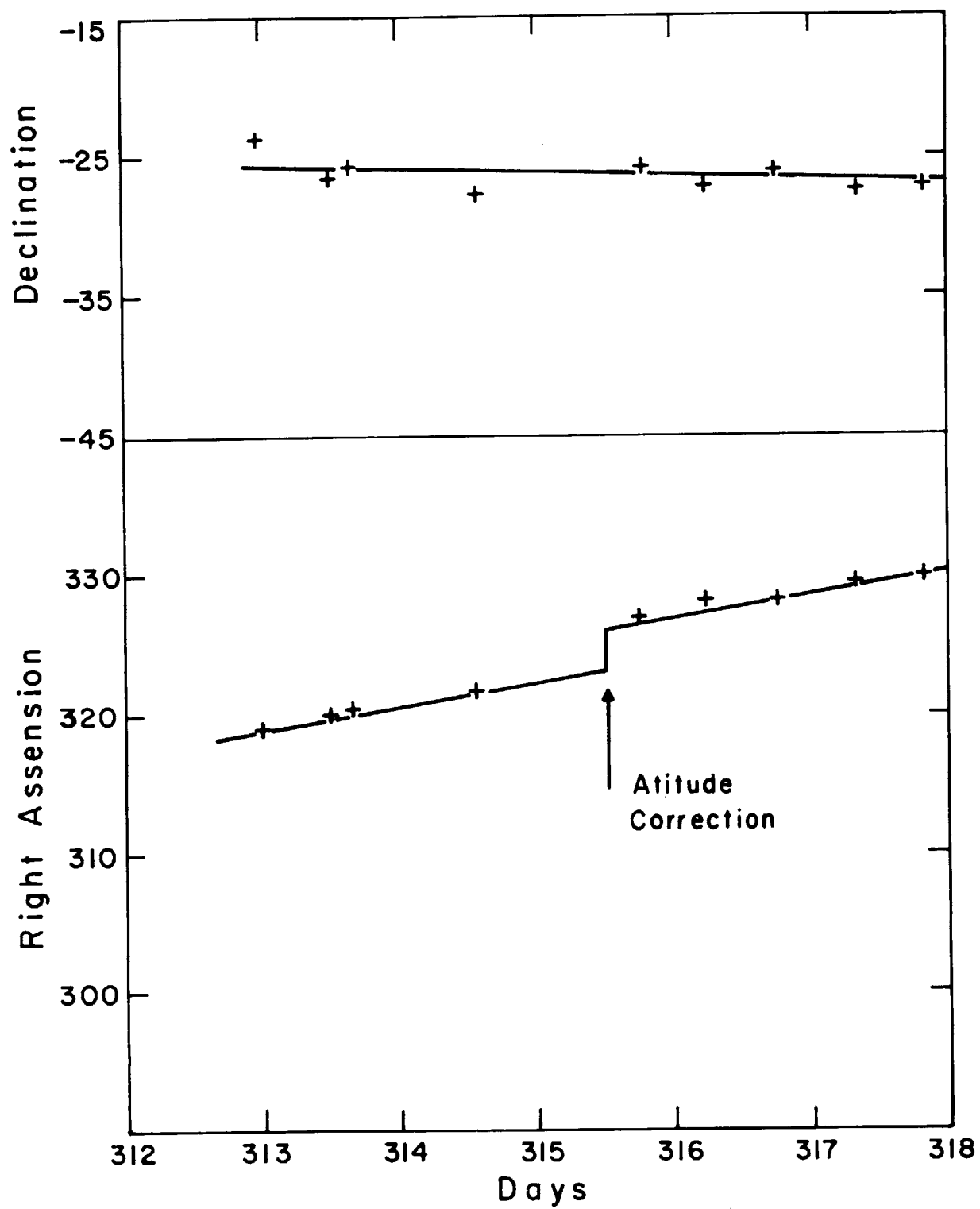


Fig. II

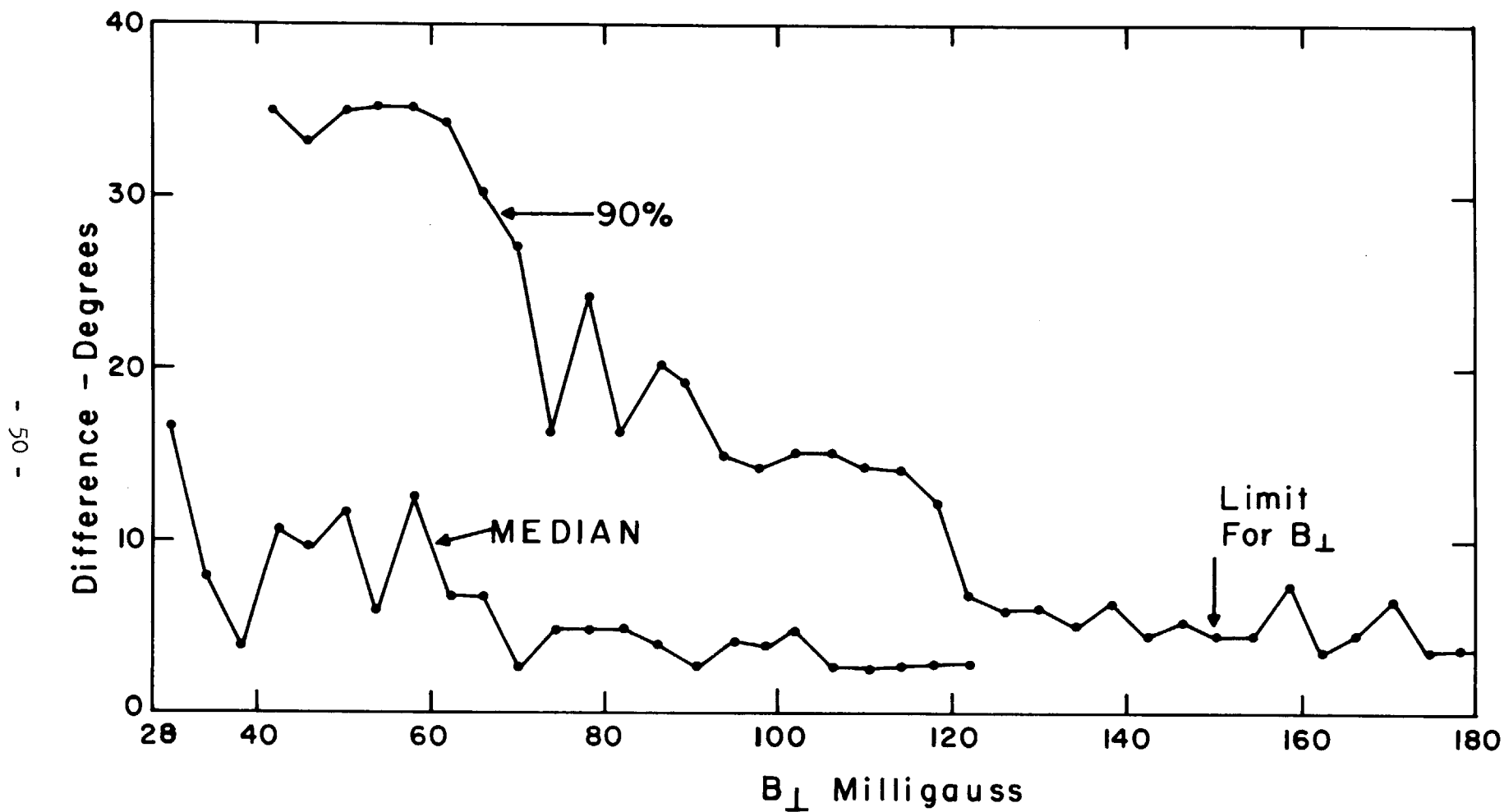


Fig. 12

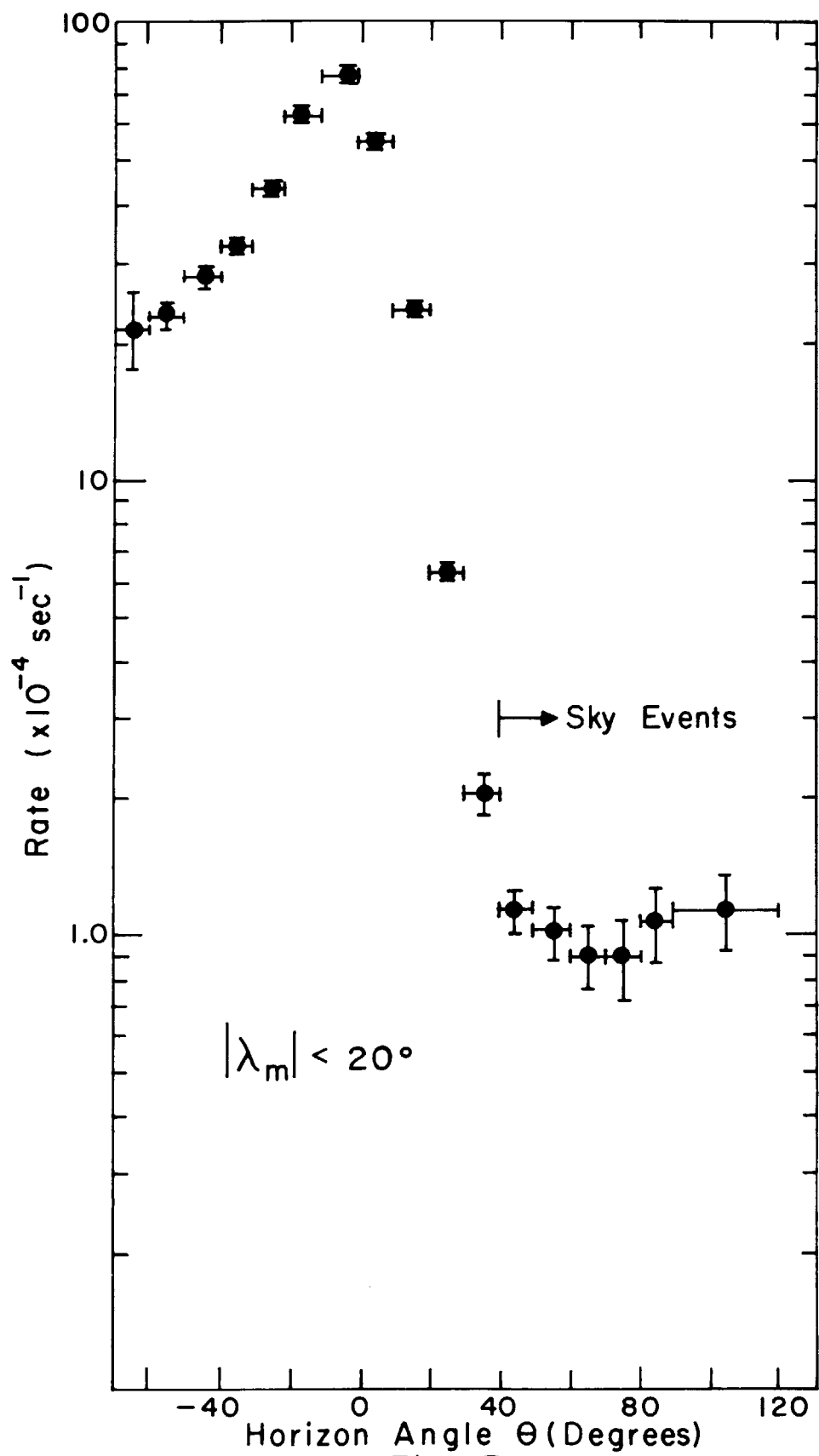


Fig. 13

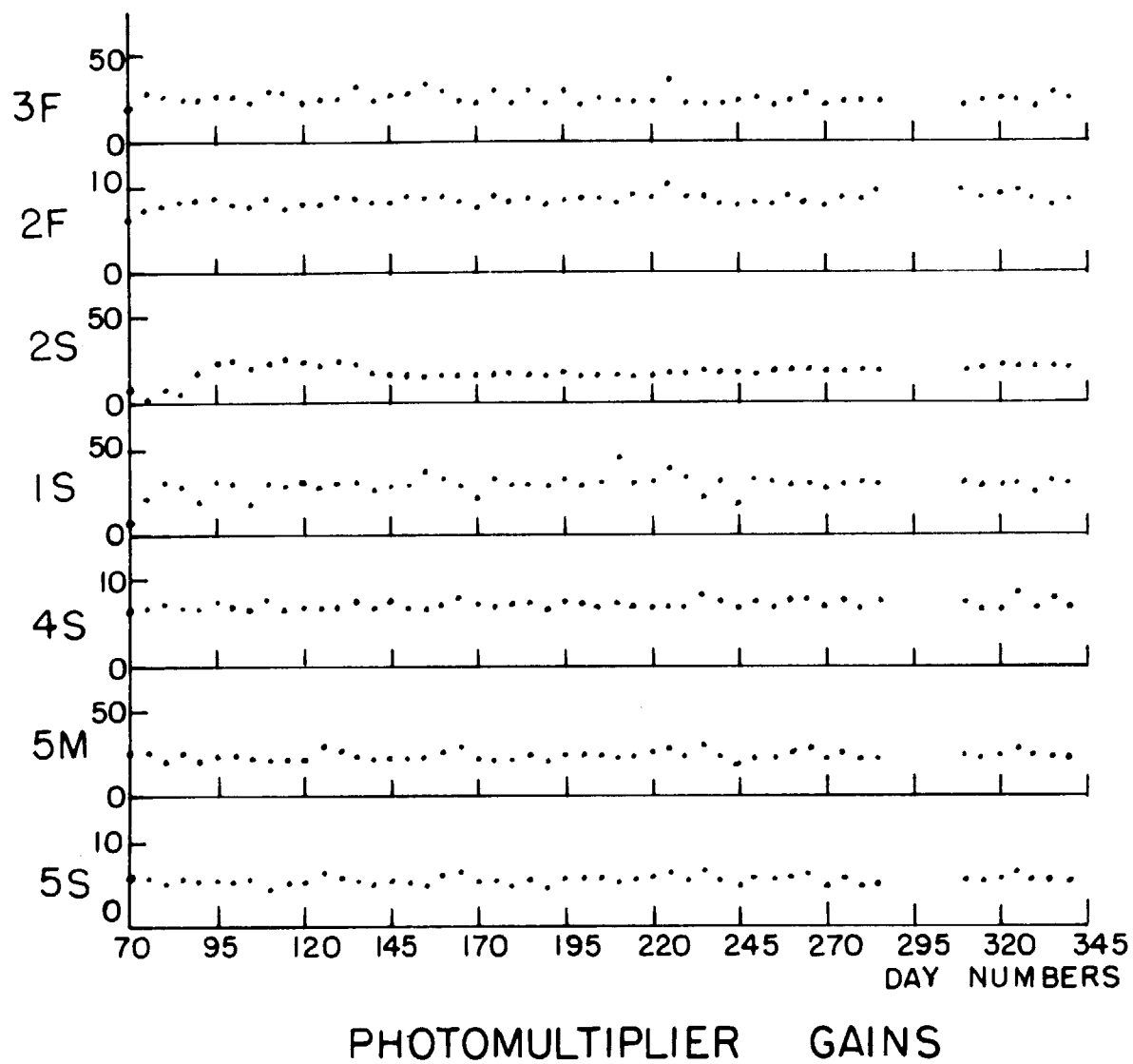


Fig. 14

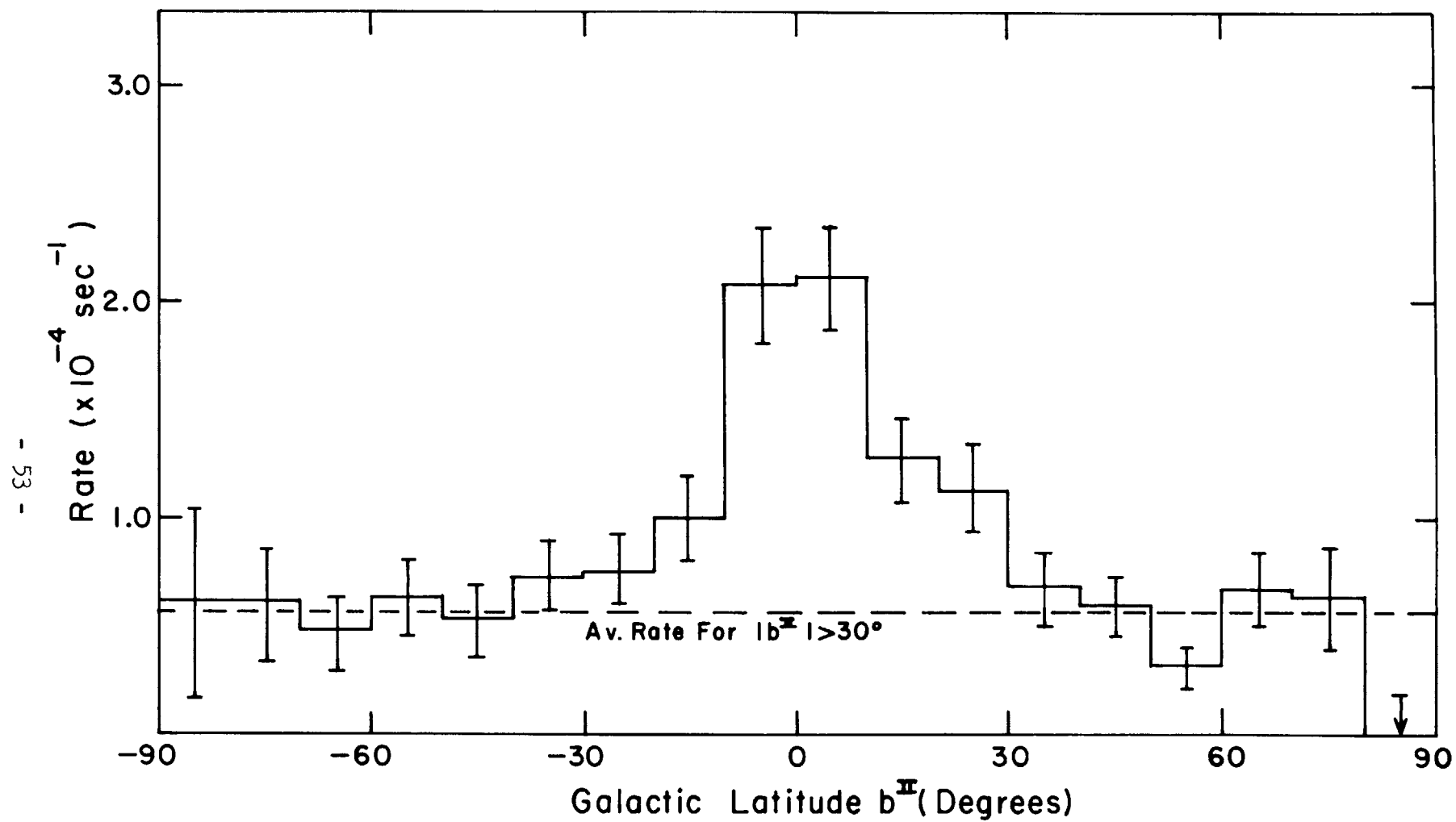


Fig. 15

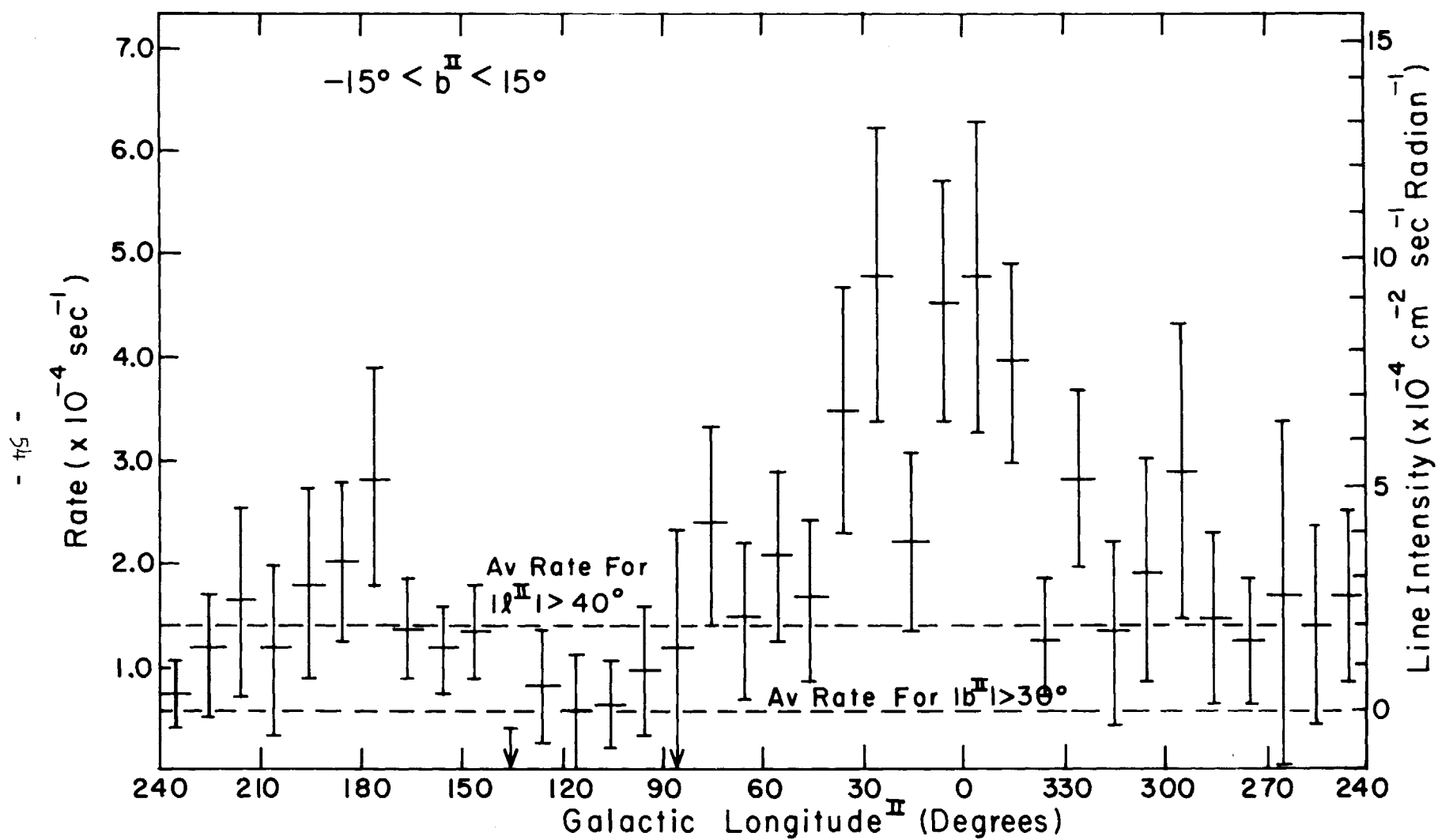
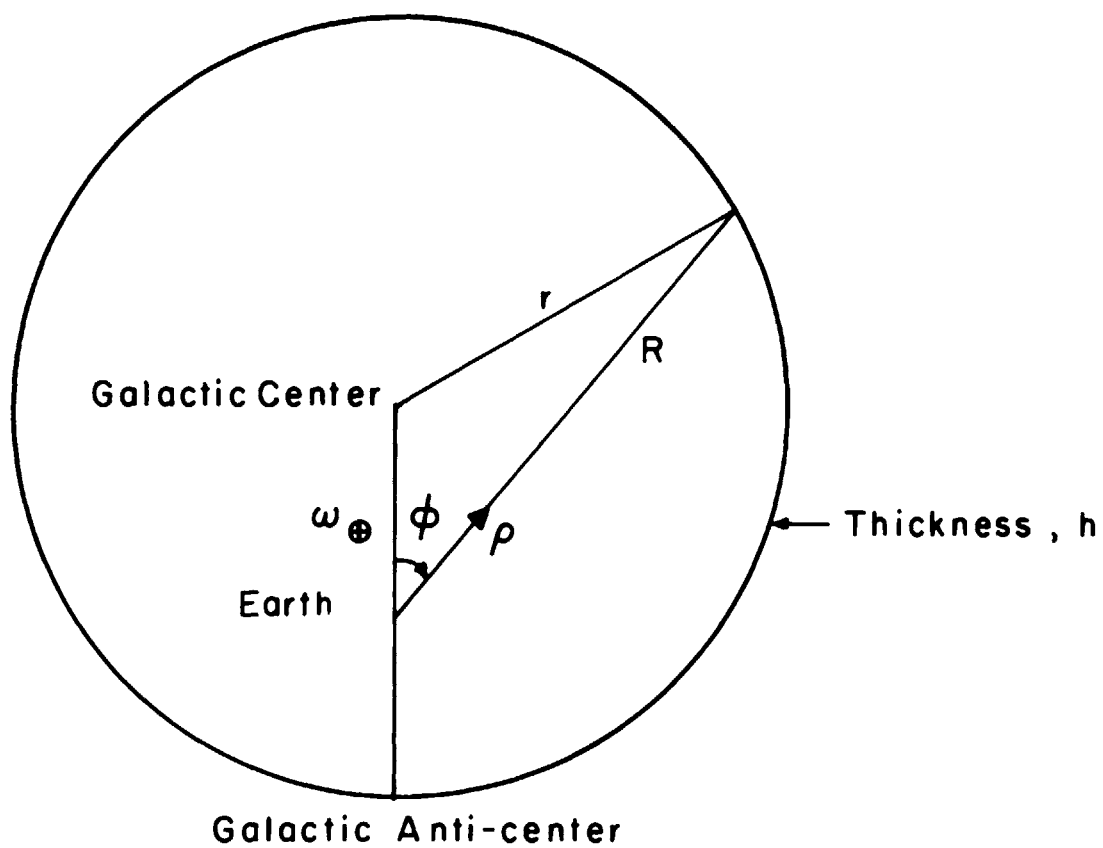


Fig. 16



Coordinate System for Calculation in Appendix

Fig.17

Table 1

Flux Upper Limits for Various Objects

Frye, Reines, and Armstrong (1966)

	$E_\gamma > 20 \text{ MeV}$	$100 > E_\gamma > 20$	$E_\gamma > 100$
Sun	$2.8 \times 10^{-2} \text{ cm}^{-2} \text{ sec}^{-1}$	2.4	2.8
M 31 (Andromeda)	1.9	1.0	1.6
Cassiopeia A	1.6	1.5	0.6
Cassiopeia B (Tycho Supernova)	1.6	1.6	1.2
M 82	1.9	1.4	1.5
Cygnus A	1.2	-	-

Fichtel and Kniffen (1965)

	$10 < E_\gamma < 50 \text{ MeV}$	$50 < E_\gamma < 200$	$E_\gamma < 200$
Sun	$1.5 \times 10^{-3} \text{ cm}^{-2} \text{ sec}^{-1}$	1.0	0.9
Taurus A (Crab Nebula)	4.2	2.9	2.8
Gemini	2.2	1.5	1.4
Spirial Arm In	8.0	5.3	5.0
Galactic Anti- center	5.1	3.5	3.4
Cygnus A	2.6	1.8	1.6

Kraushaar, Clark, Garmire, Helmken, Higbie, Agogino (1965)

	$E_\gamma > 50 \text{ MeV}$
Andromedia	$16 \times 10^{-4} \text{ cm}^{-2} \text{ sec}^{-1}$
Small Magellanic Cloud	11
Large Magellanic Cloud	9.4

Table 1 (Continued)

	$E_{\gamma} > 50 \text{ MeV}$
Taurus A	6.6
Hydra A	1.7
Virgo A	2.7
Centaurus A	3
Hercules A	3.4
Cygnus A	5
Cassiopeia A	23
Galactic center	5.3

Table 2

Symbol	Meaning
	EVENT DATA
1S	Pulse height, Slow pulse from first converter (5.7 gm/cm ² of CsI)
2S	Pulse height, Slow pulse from second converter (2.85 gm/cm ² of CsI)
2F	Pulse height, Fast pulse from second converter (.64 gm/cm ² plastic)
3F	Pulse height, Fast pulse from third converter (1.27 gm/cm ² plastic)
4S, M	Pulse height, from photomultipliers 4 and 5.
5S, M	S and M differ in gain by a ratio of 4.55:1.
MTS, MTM	number of clock cycles (at 400 cps) between the master trigger and sun or magnetometer positive zero crossing.
BLAST	Five binary bits which tell whether <ul style="list-style-type: none"> (a) The backguard counter was triggered (b) any side counters were triggered (c) If any counter was triggered 3.5 to 10 μs before a MT (d) If any counter was triggered 1.0 to 3.5 μs before a MT (e) If C was triggered (now redundant)

Table 2 (Continued)

Symbol	Meaning
--------	---------

ROUTINE DATA

Counting rates are provided at least once every 34.56 sec. for photomultipliers 1 through 15 and the following logical arrangements of counters: A + L, S·T, C, T·C, S·C, A+L+B, A (every 3.48 sec, the rudimentary telemetry cycle).

MS, SS, MM	Number of clock cycles between magnetometer sun signals, etc.
------------	---

All the above information is recorded in a digital format.

Table 3

Quantities calculated or transcribed in Pass II

Event time - accurate to 10 millisecond

Mode - gamma rays only, O/D

Event orientation - right ascension and declination of
detector axis at time of event

Satellite orientation - geographic longitude and latitude,
and altitude of the satellite

Earth orientation - the right ascension and declination of
the earth with respect to the satellite,
the angle from the detector axis to the
center of the earth, the azimuthal
angle from magnetic north around the
direction to the earth's center.

Sun orientation - celestial coordinates of the sun with
respect to the satellite.

Magnetic latitude of the satellite for an approximate dipole
representation of the earth's field.

Galactic orientation - for the event direction

Day or night flag - passed or calculated

MTS, MTM, SS, MM (cf. table 2)

The magnitude of the magnetic field lying in the plane of the
wheel.

The counting rate for the front plastic
BLAST (cf. table 2)

Pulse Heights

Table 4

	$I(\lambda_M > 20^\circ)/I(\lambda_M < 20)$
Cosmic rays	2.4 ± 0.1
Atmospheric albedo	1.40 ± 0.015
All sky events	1.05 ± 0.11
$ b^{\text{II}} > 30^\circ$	$.94 \pm 0.18$

Table 5

Direction	$N(5M \leq 10)/N(5M > 10)$
Galactic pole	2.3 ± 0.5
Galactic center	1.5 ± 0.4
Galactic anti-center	3.3 ± 1.1
Galactic plane averaged	1.9 ± 0.4

For $\lambda_M < 20$:

Horizon (east)	1.4 ± 0.12
Horizon (west)	1.9 ± 0.12
Disk of earth	5.0 ± 0.5

Table 6

 $E_\gamma > 100 \text{ MeV}$

Process	Toward:	Galactic Center	Galactic Anti-center	Galactic Pole
$\pi^0 \rightarrow 2\gamma$		$7.0 \times 10^{-5} \text{ cm}^{-2} \text{ sec}^{-1} \text{ rad}^{-1}$	$1.4 \times 10^{-5} \text{ cm}^{-2} \text{ sec}^{-1} \text{ rad}^{-1}$	$.5 \times 10^{-5} \text{ cm}^{-2} \text{ sec}^{-1} \text{ sr}^{-1}$
Inverse Compton		8.5×10^{-5}	1.3×10^{-6}	$.2 \times 10^{-5}$
Bremsstrahlung		1.2×10^{-5}	2.4×10^{-6}	1.8×10^{-6}
Metagalactic	---	---	---	10^{-5}
(Shen and Berkey)				

OSO* 4.3×10^{-4} 1.8×10^{-4} 1.1×10^{-4}

The π^0 and bremsstrahlung values were derived from the results of Ginzburg and Syrovatskii's tables (19 and 20, ref. 6) using the factor of $2 \times 10^{21} \text{ atom rad/ cm}^2$. $N(b,1) = 3.0 \times 10^{22} / (b^{1.36} + 1)$ for the integrated number density between $b = -15$ and 15 near the galactic center. (G. Garmire, private communication). The inverse Compton result was derived from that of Shen and Berkey assuming an uniform specific intensity between $b = -15$ and 15° .

* Assuming a geometric factor of $0.8 \text{ cm}^2 \text{ rad}$.